Shuffling-controlled versus strain-controlled deformation twinning: the case for HCP Mg twin nucleation

Akio Ishii

Department of Mechanical Science and Bioengineering, Osaka University, 1-3 Machikaneyama, Toyonaka, Osaka 560-8531, Japan

Ju Li*

Department of Nuclear Science and Engineering and Department of Materials Science and Engineering, Massachusetts Institute of Technology, 77 Massachusetts Avenue, Cambridge, Massachusetts, 02139, USA

Shigenobu Ogata*

Department of Mechanical Science and Bioengineering, Osaka University, 1-3 Machikaneyama, Toyonaka, Osaka 560-8531, Japan

Center for Elements Strategy Initiative for Structural Materials (ESISM), Kyoto University, Sakyo, Kyoto 606-8501, Japan

Abstract

The atomistic pathways of deformation twinning can be computed *ab initio*, and quantified by two variables: strain which describes shape change of a periodic supercell, and shuffling which describes non-affine displacements of the internal degrees of freedom. The minimum energy path involves juxtaposition of both. But if one can obtain the same saddle point by continuously increasing the strain and relaxing the internal degrees of freedom by steepest descent, we call the path strain-controlled, and vice versa. Surprisingly, we find the $\{10\bar{1}2\}\langle 10\bar{1}\bar{1}\rangle$ twinning of Mg is shuffling-controlled at the smallest lengthscale of the irreducible lattice correspondence pattern, that is, the reaction coordinate at the level of 4 atoms is dominated by non-affine displacements, instead of strain. Shuffling-controlled deformation twinning

*Corresponding authors.

Email addresses: liju@mit.edu (Ju Li), ogata@me.es.osaka-u.ac.jp (Shigenobu Ogata)

is expected to have different temperature and strain-rate sensitivities from strain-controlled deformation twinning due to relatively weaker strength of long-range elastic interactions, in particular at the twin nucleation stage. As the twin grows large enough, however, elastic interactions and displacive character of the transformation should always turn dominant.

Keywords: Civilian transformation, Military transformation, Shuffling-controlled vs. strain-controlled, Gibbs free energy landscape, Ab initio calculation of minimum energy path

---

1. Introduction

The energetics of deformation twinning (DT) has not been sufficiently clarified from first-principles, especially for the twinning systems in non-cubic and/or complex lattices, like the $\{10\bar{1}2\}\langle 10\bar{1}\bar{1}\rangle$ twinning system of HCP metals, which requires not only affine transformation strain but also non-affine atomic shuffling displacements. In this paper, we propose a rigorous mathematical definition of the strain-controlled vs. shuffling-controlled twinning at the smallest possible lengthscale (the irreducible lattice correspondence pattern) based on first-principles energetics. This approach allows us to properly define and understand the underlying mechanism and temperature/rate sensitivities of DT that accomplishes both Eshelby transformation strain and atomic shuffling, launching long- and short-ranged interaction, respectively. Moreover, some of the concepts we develop should be applicable to general solid-solid transformations, like martensitic transformations, Bainitic transformation, and the alike. We will separate the non-affine atomic shuffling with the instantaneous affine strain at the smallest lattice correspondence pattern level as the "shuffling" and "strain" variables, and compute the Gibbs free energy landscape and minimum energy path (MEP)(Jonsson et al., 1998) of DT nucleation in this joint "shuffling"-"strain" space. But if one can obtain the same MEP and saddle energy by continuously cranking just the shuffling "internal cog", and instantaneously relaxing the strain by steepest descent, we call the path "shuffling-controlled". And vice versa, if one can obtain the same MEP and saddle energy by continuously increasing the strain and relaxing the internal non-affine displacement by steepest descent, we call the path "strain-controlled".

Deformation twinning (Christian and Mahajant, 1995) transforms crystal to a mirrored configuration with transformation strain $\boldsymbol{\varepsilon}_{\text{final}}$. The basic cell

of transformation (lattice correspondence pattern), or DT supercell, can be larger than the primitive cell of the host lattice. One may represent DT atomistically by

$$\mathbf{x}_m(\lambda) = \mathbf{H}(\lambda)\mathbf{s}_m(\lambda), \;\; \mathbf{H}(\lambda) = \mathbf{R}(\lambda)(\mathbf{I} + 2\boldsymbol{\varepsilon}(\lambda))^{1/2}\mathbf{H}_0, \tag{1}$$

where λ is the reaction progress variable (scalar), $\mathbf{x}_m$ is the Cartesian position and $\mathbf{s}_m = [s_{m1}; s_{m2}; s_{m3}] \in [0, 1)$ the reduced coordinate vector of atom m under periodic boundary condition (PBC), $\mathbf{H} = [\mathbf{h}_1\mathbf{h}_2\mathbf{h}_3]$ is a 3×3 matrix where $\mathbf{h}_1$, $\mathbf{h}_2$, $\mathbf{h}_3$ are three edge vectors of the DT supercell, and $m = 1..M$ is the index of atoms in the DT supercell. $(\mathbf{I} + 2\boldsymbol{\varepsilon}(\lambda))^{1/2}$ and $\mathbf{R}(\lambda)$ is the irrotational and rotational part of the deformation gradient, respectively, where $\boldsymbol{\varepsilon}(\lambda)$ is the Lagrangian strain with respect to the initial configuration. The representation (1) is general and versatile in the sense that it can be used to represent liquid or solid geometries in molecular dynamics simulations that have general displacive and diffusive motions. Here, however, we would like to take the integer M to be as small as possible (that of the minimal, or irreducible lattice correspondence pattern) while still representing the key bonding pattern and bond-switching physics of the real DT process (Ogata et al., 2005). We believe that although DT in reality must be a heterogeneous and asynchronous transformation, the irreducible M (that is, the smallest possible lattice correspondence repeat pattern) should still give some essential, material-specific energetic information about the process. We can then compute the minimum energy path (MEP) (Jonsson et al., 1998) with the least M using parameter-free ab initio calculation at constant external stress $\boldsymbol{\sigma}$, that gives the activation Gibbs energy $G(\lambda, \boldsymbol{\sigma})$ vs. reaction coordinate λ, parametrized by $\boldsymbol{\sigma}$. This "voxel-level" activation energy profile can then be fed into mesoscale kinetic Monte Carlo (kMC) simulations, to represent large-scale thermally activated heterogeneous DT, with long-range elastic interactions between the voxels (Zhao et al., 2013). The long-range elastic interactions arise because two different voxels V and W at positions $\mathbf{x}_\mathrm{V} \neq \mathbf{x}_\mathrm{W}$ in the coarse-grained kMC simulation could be at different stages of reaction progress at any given moment

$$\boldsymbol{\varepsilon}(\lambda_\mathrm{V}) \;\neq\; \boldsymbol{\varepsilon}(\lambda_\mathrm{W}) \tag{2}$$

and such voxel-to-voxel heterogeneity in the transformation strain would cause $\propto |\mathbf{x}_\mathrm{V} - \mathbf{x}_\mathrm{W}|^{-3}$ type coupling through an elastic medium, that also determine the local stress $\boldsymbol{\sigma}_\mathrm{V}$, $\boldsymbol{\sigma}_\mathrm{W}$ by convolution (Bulatov and Argon, 1994).

We also note that such elastic interaction energy kernel is likely inaccurate when V and W voxels are adjacent to each other. Two adjacent voxels with $\{\boldsymbol{\varepsilon}_{\mathrm{V}}, \mathbf{s}_{\mathrm{V}}\}$, $\{\boldsymbol{\varepsilon}_{\mathrm{W}}, \mathbf{s}_{\mathrm{W}}\}$, where long vector $\mathbf{s} \equiv [\mathbf{s}_1; \mathbf{s}_2; ...\mathbf{s}_M]$ denotes the internal or shuffling coordinates, will likely have an interaction that depends also on $\mathbf{s}_{\mathrm{V}}$, $\mathbf{s}_{\mathrm{W}}$, and not just the strains. However, due to generalized Saint-Venant's principle, these shuffling dependent interactions are expected to decay much faster than the strain-strain interactions, so in the long range one can keep only the leading-order term which depends only on $\boldsymbol{\varepsilon}_{\mathrm{V}}$, $\boldsymbol{\varepsilon}_{\mathrm{W}}$ and not on $\mathbf{s}_{\mathrm{V}}$, $\mathbf{s}_{\mathrm{W}}$. While we will not pursue this coarse-grained simulation in detail (Bulatov and Argon, 1994; Zhao et al., 2013) in this paper, the coarse-graining concept is very important for understanding what the activation energy profile $G(\lambda, \boldsymbol{\sigma})$, computed for the least M that is still representative of the bonding energetics, means and could be useful for.

Because strain and shuffling occupy different positions in the coarse-grained total-energy framework (illustrated above for the long-range elastic interactions, which care about the strain variable only), it is critical to distinguish whether $G(\lambda, \boldsymbol{\sigma})$ is *strain-controlled* or *shuffling-controlled*. In principle one should apply algorithm to compute MEP and the saddle point of solid-solid transformation:

$$Q(\boldsymbol{\sigma}) \;\equiv\; G(\lambda^*, \boldsymbol{\sigma}) - G(0, \boldsymbol{\sigma}) \tag{3}$$

on the joint $\boldsymbol{\varepsilon} \otimes \mathbf{s}$ space (Sheppard et al., 2012), where one uses $\lambda = 0$ to denote state before transformation, $\lambda = 1$ to denote state after transformation, and λ^* for saddle-point, at constant external stress $\boldsymbol{\sigma}$. The key question is whether the MEP or reaction coordinate is dominated by $\Delta\mathbf{s}$ or $\Delta\boldsymbol{\varepsilon}$, at the minimal supercell level.

Two opposite physical limits can be identified. In the diffusive grain growth limit (e.g. annealing twin formation), $\boldsymbol{\varepsilon}_{\mathrm{final}} \approx 0$ because curvature-driven grain growth involves short-range diffusion, grain boundary motion but little strain before and after. And because of the randomized short-range diffusion that destroys labeled atom registry (if same-type, so-called "indistinguishable" atoms have labels), the lattice correspondence pattern is random and M can be taken to be ∞, so this would be a pure "shuffling-dominated" transformation with a gigantic but unchanged supercell $\mathbf{H}$. On the other hand, there are many simple metals (like FCC Cu, Au, Al and BCC Mo, Fe) that deformation-twins at low temperature with $M = 1$, where the irreducible lattice correspondence pattern (before and after DT) involves

merely one atom, evidenced by direct molecular dynamics simulations, so there is no shuffling degree of freedom and it is then purely strain-dominated. The former case is classified as civilian / diffusive transformation, the latter case is classified as military / displacive transformation (Christian, 2002), and they tend to manifest different sensitivity to temperature and strain rate (Suresh and Li, 2008; Li, 2007; Zhu and Li, 2010). The civilian / diffusive transformation tends to be more temperature and strain-rate sensitive, but less stress sensitive (less nonlinear-thresholding behavior), than military / displacive transformation, due to smaller activation volume (Li, 2007; Zhu and Li, 2010). The origin of this can in turn be traced back to the lack of long-range elastic interactions in the coarse-grained model, that tends to reduce the activation volume. Activation processes with long-range elastic interactions (Shen et al., 2008) tend to have much larger activation volume, reflecting more coordinated action across longer distances. Based on the physical reasoning above, we can state that the "voxel" strain degrees of freedom, because of the long-range elastic interaction, will always control the large-scale features of the transformation microstructure whenever $\boldsymbol{\varepsilon}_{\text{final}} \neq 0$. But regarding the thermal activation features such as temperature sensitivity, time dependence, etc., especially at the nucleation stage when the relevant lengthscale and the number of voxels involved are relatively small, the shuffling degrees of freedom could have important impact, by drawing analogy with anelasticity, diffusive creep and their relation to point defect processes whose activation volumes are small. In other words, twinning dislocations and elasticity will always become important for DT at large enough lengthscale (when the twin grows large enough)(Serra et al., 2010; Ostapovets and Molnár, 2013), but the shuffling aspect could have impact on the timescale features of the transformation kinetics. The above is actually rather general and applicable to all solid-to-solid transformations, not just twinning.

Continuum-level simulations of DT (Zecevic et al., 2015; Niezgoda et al., 2014; El Kadiri et al., 2013a; Kim et al., 2013; Oppedal et al., 2012; Proust et al., 2009; Beyerlein and Tomé, 2008) and, more generally, solid-solid transformations (Auricchio et al., 2014; Yu et al., 2013; Lee et al., 2010), have been developed and successfully demonstrate macroscopic deformation behavior. However, most of them used empirical rules to describe activation criteria of these deformation modes. Precise energetics information of $G(\lambda, \boldsymbol{\sigma})$ based on ab-initio density functional theory (DFT) should be very useful for these continuum-level simulations. Recently, atomic-level analyses by molecular dynamics are also reported (Wang et al., 2014; Luque et al., 2014; Wang

et al., 2013a,b; Luque et al., 2013; Li et al., 2012; Wang et al., 2009a,b; Li and Ma, 2009a,b). However, atomic energetics information along the DT minimum energy path (including shuffling component) in HCP Mg has not been reported. Detailed analysis of shuffling depends on the crystallographic analyisis(Kihô, 1954; Bilby and Crocker, 1965; El Kadiri et al., 2013b; Khater et al., 2013). Recently, Luque et al. proposed mathematical model which can deal with twin nucleation and growth with solute atoms (Luque et al., 2014). Although twin boundary misfit energy is determined by DFT calculation in their paper, the activation energy of twin nucleation is determined empirically because of the lack of ab initio energetics. Motivated by this, we decide to study whether DT in hexagonal close-packed (HCP) magnesium is *strain-controlled* or *shuffling-controlled* by ab initio DFT calculation. We note that even though the Bravais primitive cell of HCP metals contains only $N = 2$ atom, because of the lower symmetry of twinning system, M can be larger than 2, which should be an integer multiple of N in general.

2. Mathematical definition of the strain-controlled vs. shuffling-controlled concept for solid-solid transformation

We give a precise and general mathematical definition of the *strain-controlled* vs. *shuffling-controlled* concept for solid-solid transformation as follows. Generally, the energy landscape of M-atom supercell can be defined in $3M + 6$ dimensional space, $[\boldsymbol{s}, \boldsymbol{\varepsilon}]$. $\boldsymbol{s}$ is the internal coordinates of labeled atoms ($3M$ dimensions) and $\boldsymbol{\varepsilon}$ is the supercell strain tensor (6 dimensions) with respect to a prescribed reference.

We will use a scalar γ to represent progress in $\boldsymbol{\varepsilon}$. In the case of a simple-shear dominated $\boldsymbol{\varepsilon}$, γ is chosen to be the dominant engineering shear strain component.

$$\gamma \equiv 2\varepsilon_{yz} \tag{4}$$

where z is the K_1 invariant plane normal, and y is the $K_2 \rightarrow K_2'$ shear displacement direction of DT (Christian and Mahajant, 1995). By definition, $\gamma = 0$ when $\lambda = 0$. We can then increase γ a little and fix it as a constraint, and then relax the remaining $3M+5$ degrees of freedom in ab initio supercell calculation by steepest descent method. And then one repeats the process. If we can reach the same activation energy $G(\lambda^*)$ as the full $\boldsymbol{\varepsilon} \otimes \mathbf{s}$ minimum energy path search by trotting along γ, we will call this activation path strain-controlled, in the sense that the reaction coordinate can be pretty well

represented by γ. On the other hand, let us also define a scalar to represent the shuffling degree of freedom. We will choose:

$$I \equiv (\boldsymbol{s} - \boldsymbol{s}^{\text{ini}})^T \mathbf{H}_0^T \mathbf{H}_0 (\boldsymbol{s}^{\text{fin}} - \boldsymbol{s}^{\text{ini}})/M \tag{5}$$

where $\boldsymbol{s}^{\text{ini}}$ is the internal coordinates of labelled atoms before twinning ($\lambda = 0$), and $\boldsymbol{s}^{\text{fin}}$ is the internal coordinates of labelled atoms after twinning ($\lambda = 1$), for a given $\boldsymbol{\sigma}$. Please note that the $\boldsymbol{s}$ differences in (5) are the changes in internal coordinate *without* PBC wrap-around, same as how the atomic mean-square displacement (MSD) is computed in PBC. I has the unit of Å^2 and takes the meaning of the mean-square non-affine displacements (MSD) when the solid-solid transformation finishes. By definition, $I = 0$ when $\lambda = 0$. One can do an alternative calculation where one increases I a little and fix it as a constraint variable, and relax the remaining $3M + 5$ degrees of freedom by steepest descent, and then repeat trotting along I. In this case, all 6 strain tensor components become "slaved" variables of I: the supercell shape and size respond instantaneously to the tweaking of this internal "cog". If we can get to the same saddle point $G(\lambda^*)$ as the full $\boldsymbol{\varepsilon} \otimes \mathbf{s}$ path search, we will call this activation path shuffling-controlled, in the sense that the reaction coordinate can be pretty well represented by I. If neither γ-control or I-control can give us the right saddle energy, or if both can, we will call such transformation path as under *mixed*-control.

3. Non-basal $\{10\bar{1}2\}\langle 10\bar{1}\bar{1}\rangle$ deformation twinning in HCP magnesium

HCP magnesium alloys are promising lightweight structural materials. Hampering broader applications, however, is the limited formability of HCP Mg which originates from its plastic anisotropy. This is because the slip (or twinning) systems of HCP Mg are not equivalent and the critical resolved shear stress (CRSS) can differ greatly. In HCP Mg single crystal, basal slip has the lowest CRSS, 0.5-5MPa (Akhtar and Teghtsoonian, 1969a; Chapuis and Driver, 2011) at room temperature. On the other hand, the non-basal slip and twinning systems, which can produce deformation along the c-axis, have a much higher CRSS (Chapuis and Driver, 2011). For example, 20-30MPa of prismatic slip (Akhtar and Teghtsoonian, 1969b; Yoshinaga and Horiuchï, 1963), 6-10MPa of $\{10\bar{1}2\}\langle 10\bar{1}\bar{1}\rangle$ twinning system have been reported(Kelley and Hosdord, 1968; Chapuis and Driver, 2011). Although con-

siderable research has been devoted to improving the formability and understanding the plastic anisotropy both experimentally and theoretically, much uncertainties remain. Among these, non-basal $\{10\bar{1}2\}\langle 10\bar{1}\bar{1}\rangle$ DT is presently receiving much attention, because DT frequently appears as a result of the high Schmid factor of $\sim$0.5 when tensile normal stress exists perpendicular to the basal plane (Luque et al., 2013). Many experimental studies and theoretical analyses have been performed on the HCP $\{10\bar{1}2\}\langle 10\bar{1}\bar{1}\rangle$ twinning system.

Nevertheless, information regarding the required mechanical conditions and atomistic twinning processes is still not fully clarified. For example, recent nano-sample uniaxial extension (or compression) experiments show quite higher CRSS, 400MPa (Yu et al., 2012) or 250MPa (Liu et al., 2014), compared with previous bulk CRSS value, 6-10MPa(Kelley and Hosdord, 1968; Chapuis and Driver, 2011), due to size effect on plasticity like for other non-basal slip systems (Byer and Ramesh, 2013; Lilleodden, 2010), that may be attributable to the increased importance of DT nucleation (vs DT growth) in small samples (Zhu and Li, 2010). The non-Schmid effect is also reported for HCP Mg secondary $\{10\bar{1}2\}\langle 10\bar{1}\bar{1}\rangle$ twin (Barnett et al., 2008), Zr, Ti polycrystal compression experiment (Capolungo et al. , 2009; Wang et al., 2010) and molecular dynamics study (Barrett et al. , 2012). Moreover, in Mg and Ti, recent TEM analysis show the existence of the incoherent $\{10\bar{1}2\}\langle 10\bar{1}\bar{1}\rangle$ twin boundary, Basal-Prismatic (BP) or Prismatic-Basal (PB) boundaries, and faceting of twin boundary(Wang et al., 2013a; Tu et al., 2013; Liu et al., 2014; Barrett and El Kadiri, 2014a,b; Sun et al., 2015; Tu et al., 2015). The reasons for these unique properties are not clear and we think shuffling could be a factor for consideration. Non-schmid effect and the BP,PB interfaces seems to be partially thermal activated rather than purely stress (or strain) driven. For example, Liu et al. observed BP, PB in their nano-pillar compression test (Liu et al., 2014), where the loading direction is normal to c-direction and the resolved shear stress along BP and PB are small. This may suggest the nucleation or growth of BP and PB boundaries is not purely controlled by the direction of stress, and thermally activated shuffling could be important (although the magnitude of the stress is also important).

Our study aims to provide a DFT-based Gibbs energy landscape of $\{10\bar{1}2\}\langle 10\bar{1}\bar{1}\rangle$ DT. Figure 1 shows perfect ($\lambda = 0$) and twinned ($\lambda = 1$) HCP atomic structures viewed from $\langle 1\bar{2}10\rangle$, at $\boldsymbol{\sigma} = 0$. The four-atom parallelepiped supercell used in this study, which includes atoms A, B, C, and D, is indicated as a

broken red line. The four-atom supercell ($M = 4$) is the minimum lattice correspondence pattern unit necessary to render the atomic arrangements during $\{10\bar{1}2\}\langle 10\bar{1}\bar{1}\rangle$ twinning shear deformation (Li and Ma, 2009a; Wang et al., 2013b). This deformation pattern in our definition is the same as the one proposed based on crystallographic analysis(El Kadiri et al., 2013b; Khater et al., 2013; Bilby and Crocker, 1965). Our repeat unit expresses 2-layer zonal DT. The twin thickness and twin dislocation correspond to h_2 and $\boldsymbol{b}_2$ in (Khater et al., 2013; Bilby and Crocker, 1965) and the change of I corresponds to the net shuffles without any plastic deformation(El Kadiri et al., 2013b).

Here we should note again that our DFT model cannot evaluate the realistic twin nucleation and twin growth quantitatively. Realistic DT will be heterogenous, say initially twin embryo is nucleated (twin nucleation), then twin boundary will migrate (twin growth). With DFT calculation, it is difficult to deal with the heterogeneity due to computational cost. In larger scale atomistic calculations like MD, we can deal with such heterogenous deformation and its total energetics(Rasmussen et al., 1997; Sheppard et al., 2012), but everything will be based on empirical interatomic potential usually. In this paper, we try to reduce the problem to a manageable complexity with DFT, and then use kMC to do the coarse-graining which will include the elastic field of the twinning dislocations in the future, that should be able to handle both twin nucleation and growth (Shen et al., 2008).

4. Methods

We employed the Vienna *ab-initio* simulation package (VASP) (Kresse and Furthmüller, 1996) with a Perdew-Wang generalized gradient approximation functional (Perdew et al., 1992) and projector-augmented wave potentials (Kresse and Joubert, 1999) for Mg ($3s^2 3p^0$ valence). An energy cutoff of 265 eV was used for the plane wave expansion. A Monkhorst-Pack **k**-point mesh (Monkhorst and Pack, 1976) of $13 \times 13 \times 13$ was used, which reduces **k**-point sampling error to less than 1.0 meV/Å. The energy convergence criteria of the electronic and ionic structure relaxations were set to 10^{-9} and 10^{-3} eV, respectively. For the electronic structure relaxation, the RMM-DIIS algorithm (Pulay, 1980) was used. The computed HCP lattice parameters are a_0/c_0 =1.628, a_0 =3.195 Å and the shear modulus G for the twinning shear mode is 19.5 GPa. These values are in reasonable agreement with those obtained in other theoretical studies (a_0/c_0 =1.628 (Nie and Xie, 2007;

Sandlöbes et al., 2012) and a_0 =3.13 Å (Nie and Xie, 2007)) and experimental measurements(a_0/c_0 =1.624 (Yoo, 1981), a_0 =3.209 Å (Yoo, 1981) and G =21.49 GPa (Ogata et al., 2004)) . Subroutines of independent stress and strain component control (Ogata et al., 2005) and atomic and supercell shape relaxation under constraints (drag method (Jonsson et al., 1998)) have been implemented into the VASP code. In our DFT results we have not considered the vibrational entropy contribution to G at finite temperature (although in principle we could by performing harmonic expansion), so our results can be considered the enthalpic contribution or the $T \to 0$K limit of the Gibbs free energy landscape.

5. Results and discussion

We first evaluate the internal energy U of the supercell with respect to the uniform twinning shear deformation,

$$U(\gamma) \;=\; \min_{\mathbf{s},\boldsymbol{\varepsilon}\in\gamma} U(\boldsymbol{\varepsilon},\mathbf{s}) \tag{6}$$

and these are shown in Fig. 2 (a) and (b). The shear deformation was applied to two different fully relaxed HCP supercells, which have HCP and twinned HCP configurations. We termed these supercells "original" (red plots in Fig. 2 (a) and (b)) and "twinned" (green plots in Fig. 2 (a) and (b)). Both of these supercells have the same perfect HCP lattice structure, but the twinned supercell has the sheared supercell frame from the original supercell of $\gamma = \gamma_{yz}$ =0.124 engineering shear strain. We should note that internal atomic configurations in these supercells can be different even though they have the same supercell shape. We actually found the internal atomic configuration $\mathbf{s}$ at a certain engineering shear strain to be dependent upon whether it has been sheared from the "original" or the "twinned" supercell. It causes internal energy and stress differences at each engineering strain γ, shown as the red and green plots in Fig. 2 (a) and (b). In Fig. 2 (a), there exists an energy crossover at a critical $\gamma = \gamma_{\rm c}$ (= 0.062) between these plots. Above the critical strain, an atomic configuration sheared from a twinned supercell becomes energetically favorable compared to that of the original supercell with the same cell shape, and thermodynamics would start to allow DT to happen at T = 0 K. However, even at a little above the critical strain, a transition from red to green curve in Fig. 2 (a) and (b) still seem to involve an energy barrier. In other words, spontaneous twinning

has not been observed in the DFT calculation, in the absence of thermal fluctuations and waiting times. This already hints that the twinning shear strain γ may not be the dominant reaction coordinate. There is something internal that "got stuck" and pegs the red→green transition from happening spontaneously, even quite above the equi-energy strain γ_c.

To examine the "internal cog" effect in detail, we define and numerically evaluate the Gibbs free energy landscape using ab initio supercell energetics

$$G(\boldsymbol{\varepsilon}, \boldsymbol{s}, \boldsymbol{\sigma}) \equiv U(\boldsymbol{\varepsilon}, \boldsymbol{s}) - W(\boldsymbol{\varepsilon}, \boldsymbol{\sigma}), \tag{7}$$

where $W(\boldsymbol{\varepsilon}, \boldsymbol{\sigma})$ is the work done by constant external Cauchy stress $\boldsymbol{\sigma}$ (Wang et al., 1995):

$$\begin{aligned} W(\boldsymbol{\varepsilon}, \boldsymbol{\sigma}) \equiv & \int_0^1 dl \det |\mathbf{J}(\boldsymbol{\eta} = l\boldsymbol{\varepsilon})\mathbf{H}_0| \\ & \times \mathrm{Tr}\left[\mathbf{J}^{-1}(\boldsymbol{\eta} = l\boldsymbol{\varepsilon})\boldsymbol{\sigma}\mathbf{J}^{-T}(\boldsymbol{\eta} = l\boldsymbol{\varepsilon})\boldsymbol{\varepsilon}\right], \end{aligned} \tag{8}$$

where $\boldsymbol{\eta} = l\boldsymbol{\varepsilon} = 1/2(\mathbf{J}^{\mathrm{T}}\mathbf{J} - \mathbf{I})$ is the Lagrangian strain tensor, $\mathbf{J}$ is the corresponding deformation gradient tensor:

$$\mathbf{J} = \mathbf{R}(\mathbf{I} + 2\boldsymbol{\eta})^{1/2} \tag{9}$$

and $\mathbf{R}$ is an additional rotation matrix $\mathbf{R}^T\mathbf{R} = \mathbf{I}$ that is completely defined when the transformation coordinate frame convention is chosen.

Even though $G(\boldsymbol{\varepsilon}, \boldsymbol{s}, \boldsymbol{\sigma})$ is now defined by (7), since $\boldsymbol{\varepsilon} \otimes \mathbf{s}$ space is $3M + 6$ dimensional, it is difficult to be visualized directly. So we can use (4) and (5) to help the visualization. By applying energy minimization to all degrees of freedom of the supercell system other than γ and I, we can uniquely compute $G(\gamma, I, \boldsymbol{\sigma})$:

$$G(\gamma, I, \boldsymbol{\sigma}) \equiv \min_{\boldsymbol{\varepsilon} \in \gamma, \boldsymbol{s} \in I} G(\boldsymbol{\varepsilon}, \boldsymbol{s}, \boldsymbol{\sigma}) \tag{10}$$

The computed Gibbs energy landscapes $\Delta G(\gamma, I)$ at different external Cauchy shear stresses, $\sigma_{yz} = \sigma_{zy} = 0$ GPa, 1 GPa, and 2 GPa along the twinning direction, are shown in Fig. 3. The other Cauchy stress components were set to zero. The red curves on the Gibbs energy landscapes represent the minimum energy paths (MEPs) from the original to the twinned configuration under these external shear stresses, which were estimated by applying the nudged elastic band (NEB) method (Jonsson et al., 1998) to obtain the two-dimensional Gibbs energy landscapes. The MEP analysis based on

the Gibbs energy landscape clearly indicates that a uniform supercell shape change and an atomic position change simultaneously happen during the DT process. Figure 4 represents the atomic position change along the MEP at 0 GPa shear stress. A "dumbbell flipping" or "shuffling", that is, staggered rotations of the A-B and C-D atomic bonds, behavior can be seen together with a uniform supercell shear deformation (see also supplemental movie (Suppl_movie.pptx)). The Gibbs energy change along the MEP under different external shear stresses is shown in Fig. 5 (a), and Fig. 5 (b) shows the change in the Gibbs energy barrier with respect to the external shear stress.

We also independently performed the following two kinds of NEB calculations: (1) an NEB calculation with respect to the internal atomic configuration I, in which the supercell frame is relaxed under the predefined external stress (I-control NEB). (2) an NEB calculation with respect to γ, in which internal atomic configuration $\mathbf{s}$ is relaxed for each supercell frame shape (γ-control NEB). A comparison between two-dimensional Gibbs energy landscape, I-control NEB and γ-control NEB Gibbs energy barriers is presented in Fig. 5(b), and one can find that the Gibbs energy barrier determined by I-control NEB agrees well with the Gibbs energy barrier based on the two-dimentional Gibbs energy landscape, whereas the Gibbs energy barrier obtained by the γ-control NEB is significantly higher. This indicates that the DT is an I-dominant (non-affine displacement dominant) deformation at the smallest lengthscale of the irreducible lattice correspondence pattern. Thus, if an assist of thermal energy were to exist (say by a rare event of 20 phonons colliding within one voxel), the twinned structure could be generated without generating local shear strain, as the phonons could toggle the "internal cog" of the voxel. Once the "internal cog" is flipped, the voxel γ will spontaneously relax toward the twinned configuration later.

Wang et al. also calculated the stress and potential energy versus uniaxial c-direction extension strain of the $M = 4$ atoms unit cell with DFT (Wang et al., 2013b). The critical stress and activation energy of uniform deformation can be estimated from their plot. The difference with our work is that they did not treat strain and shuffling degrees of freedom equally, and their model is similar to our γ-control NEB. Actually, because of this, they overestimated the activation energy; their value is higher than our activation energy at 0GPa, 17meV/atom.

Another point we should mention is that the DT is not totally insensitive to stress even though it is I-dominant. Figure 5(b) shows that the Gibbs energy barriers of all cases decrease with increasing applied external shear

stress, but the dependency of I-control NEB and two-dimentional Gibbs energy landscape case is weaker than the γ-control NEB case. Originally, shuffling is regarded as strain free (Kihô, 1954). However, our calculations show that plastic deformation follows spontaneously and strain is induced once shuffling occurs (Li, 2004). Thus we cannot divide strain and shuffling perfectly, as they are not "orthogonal". Even though the shuffling degree of freedom I is the controlling variable in our DFT MEP, the strain is slaved to the shuffling, and therefore the shuffling energy landscape is also biased by the external stress. So stress influences the energy landscape in all situations.

There exists a gray zone between pure "deformation twinning" (DT) and pure "annealing twinning" (AT), and our work aims to quantify this grayness. For "annealing twinning", diffusive thermally activated processes control the twinning. In AT, the transformation strain (based on experimental metallography of tracking fiducial markers on sample) is zero, relative to which the shuffling mean square displacement is obviously significant. (Mao et al., 2015; Li et al., 2015) In contrast, in the textbook example of diffusionless DT of FCC metals, the transformation strain is huge (like 70.7%), but shuffling MSD is assumed to be zero (although there are complications like random activation of partials (RAP) twinning in FCC metals (Wu et al., 2008; Zhu et al., 2012) also). In our case of Mg $\{10\bar{1}2\}\langle 10\bar{1}\bar{1}\rangle$ DT, the transformation strain is relatively small, only 12.4%, and the shuffling degrees of freedom does account for much of the action within the $M = 4$ repeat unit. So our case falls squarely in the gray zone.

Eventually an athermal condition is achieved at a critical external shear stress of $\sim$3.0 GPa. Thus, applying 3.0 GPa external shear stress can induce the DT regardless of the internal atomic configuration I. So DT becomes γ-dominant (shear strain induced) under such an extremely high shear stress. CRSS=3.0GPa corresponds to ideal strength for DT, which can be achieved only if without any pre-existing defects (not even surfaces), and without any thermal activation (T=0K) (Zhu and Li, 2010). This can be used as a reference value to normalize local stress and assess whether a voxel-level local stress is "high" or "low". Twin nucleation could be shuffle-controlled when the embryo is small and voxel-level local stress is "low". Twin dislocations and elasticity will become more important as the twin grows bigger because voxel-level local stress at twin tip gets progressively higher due to load shedding from a larger region. For the quantitative analysis, again, we are building the kMC model with long-range voxel-to-voxel elastic interactions, (Zhao et al., 2013) to represent strain-carrying defects like the twin

dislocations. (Shen et al., 2008)

Having said that, for twin nucleation at room temperature, it should be very unlikely to find as high shear stress as CRSS=3.0GPa due to the existence of thermal energy. We believe that in a practical load-ramp experiment at room temperature, where a typical applied strain rate is 10^{-3}/s, there is enough time and thermal fluctuations that the system would undergo DT with shuffling-controlled thermal activation path, as the voxel passes the low- and intermediate stress regime before it ever reaches the extremely high-stress regime. In other words, we believe that local atomic shuffling does dominate Mg's $\{10\bar{1}2\}\langle 10\bar{1}\bar{1}\rangle$ twinning at room temperature and normal strain rates, from ab initio energetics perspective (Li and Ma, 2009a; Wang et al., 2013b; Li and Zhang, 2014). Based on our preliminaly kMC calculations at T=300K, local twin nucleation stress could be as high as 400MPa, in reasonable agreement with recent nano-pillar extension test (Yu et al., 2012).

We also examined changes in the other strain components during the twinning shear process along the MEP (Fig. 6). Finite negative normal engineering strains (contractions) up to -1.0 % in ε_{yy} and ε_{zz} and positive (extensions) up to 2.4 % in ε_{xx} were observed at the saddle point. This suggests that tensile stress σ_{xx}, and compressive stresses σ_{yy} and σ_{zz} may help the DT (Ogata et al., 2002).

Barrett et al. (2012) observed lower CRSS of $(\bar{1}102)$ twinning system with $[10\bar{1}2]$ uniaxial extension than that of the equivalent $(10\bar{1}2)$ twinning system with [0001] uniaxial extension. With $[10\bar{1}2]$ uniaxial extension, not only the shear strain, but the positive ε_{xx} is also provided to $(\bar{1}102)$ twinning system, which helps the DT according to our result. On the other hand, [0001] uniaxial extension gives negative ε_{xx} to $(10\bar{1}2)$ twinning system, which suppresses the DT according to our ab initio energetics. So our ab initio energetics along MEP is consistent with the observed non-Schmid effect of (Barrett et al. , 2012). It is worth noting that once DT grows large enough, the shear stress along the transformation strain direction will play the dominant part of the driving force of the twin growth as we mentioned in the previous section. Thus, Schmid's law should work better in that limit.

6. Conclusion

In summary, we have given a proper mathematical definition to the voxel-level reaction progress variable of local solid-state transformation, to be

"affine" (strain-controlled) or "non-affine" (shuffling-controlled). Applying our analysis to Mg $\{10\bar{1}2\}\langle 10\bar{1}\bar{1}\rangle$ DT, the Gibbs energy landscape of Mg $\{10\bar{1}2\}\langle 10\bar{1}\bar{1}\rangle$ twinning shear was derived based on first-principles density functional theory. Using the Gibbs energy landscape, we figured out the MEPs of the twinning shear processes under various external local shear stress conditions, and the Gibbs energy, shear strain, and atomic configuration changes along the MEPs were computed. Knowing the data along the MEPs allows us to know the athermal shear stress of 3.0 GPa for the uniform twinning shear deformation; moreover, a "dumbbell flipping" or "shuffling" atomic motion together with uniform shear strain was found to be a deformation pathway of the twinning shear.

We conclude that Mg $\{10\bar{1}2\}\langle 10\bar{1}\bar{1}\rangle$ DT is likely dominated by local atomic shuffling at room temperature and normal strain rates at the nucleation stage. The stress dependency is relatively small (but still exists). Thus, it should have a relatively small activation volume, and more sensitive dependencies on temperature and applied strain rates, than the typical DT processes in FCC and BCC metals that are strain-controlled and have stronger elastic interactions due to the much larger transformation strains.

Finally we note that the present work is still incomplete, in the sense that the ab initio energetics needs to be brought to larger length scales, which we plan to do with the kMC model in a follow-up work. "Shuffle-controlled" vs. "strain-controlled" mentioned in the paper are at the level of the smallest possible length scale, that of the $M = 4$ repeat cell. This should not directly translate to "shuffle-controlled" vs. "strain-controlled" at the larger mesoscale level where strain-induced elastic interactions could become more prominent and important, although with a "grayness" from small to larger lengthscales. From our result, there is always stress sensitivity, as stress influence both our affine and deterministically non-affine displacements. At mesoscale, "shuffle-controlled" is likely to be true at smaller lengthscales such as twin nucleation. But as the deformation twin grows big, long-range elastic interactions and strain-carrying defect will bias more toward "strain-controlled" twin propagation (manifesting as larger activation volume, lower temperature and strain-rate sensitivities in the propagation stress).

Acknowledgements

AI acknowledges support by KAKENHI Grant No. 25·2497 (JSPS fellowship). SO acknowledges support by KAKENHI Grant Nos. 23246025

(Scientific Research (A)), 22102003 (Scientific Research on Innovative Area), and 25630013 (Challenging Exploratory Research), and Elements Strategy Initiative for Structural Materials (ESISM). JL acknowledges support by NSF DMR-1410636 and DMR-1120901. AI thanks Prof. Hajime Kimizuka and Prof. Yunjiang Wang for fruitful discussions.

References

Akhtar, A., Teghtsoonian, E., 1969a. Solid solution strengthening of magnesium single crystals-I alloying behaviour in basal slip. Acta Metall. 17, 1339–1349.

Akhtar, A., Teghtsoonian, E., 1969b. Solid solution strengthening of magnesium single crystals-II the effect of solute on the ease of prismatic slip. Acta Metall. 17, 1351–1356

Auricchio, F., Bonetti, E., Scalet, G., Ubertini, F., 2014. Theoretical and numerical modeling of shape memory alloys accounting for multiple phase transformations and martensite reorientation. Inter. J. Plas. 59, 30–54.

Barrett, C. D., El Kadiri, H., Tschopp, M. A., 2012. Breakdown of the Schmid law in homogeneous and heterogeneous nucleation events of slip and twinning in magnesium. J. Mech. Phys. Sol., 60, 2084–2099.

Barnett, M., Keshavarz, Z., Beer, A., Ma, X., 2008. Non-Schmid behaviour during secondary twinning in a polycrystalline magnesium alloy. Acta Mater. 56, 5–15.

Barrett, C. D., El Kadiri, H., 2014a. Impact of deformation faceting on $\{10\bar{1}2\}$, $\{10\bar{1}1\}$ and $\{10\bar{1}3\}$ embryonic twin nucleation in hexagonal close-packed metals. Acta Mater. 70, 137–161.

Barrett, C. D., El Kadiri, H., 2014b. The roles of grain boundary dislocations and disclinations in the nucleation of $\{10\bar{1}2\}$ twinning. Acta Mater. 63, 1–15.

Beyerlein, I. J., Tomé, C. N., 2008. A dislocation-based constitutive law for pure Zr including temperature effects. Inter. J. Plas. 24, 867–895.

Bilby, B. A., Crocker, A. G., 1965. The Theory of the Crystallography of Deformation Twinning. Proc. Royal Soc. A: Math. Phys. Eng. Sci. 288, 240–255.

Bulatov, V. V., Argon, A. S., 1994. A stochastic model for continuum elasto-plastic behavior. I. Numerical approach and strain localization. Modell. Sim. in Mater. Sci. Eng. 2, 167–184.

Byer, C. M., Ramesh, K., 2013. Effects of the initial dislocation density on size effects in single-crystal magnesium. Acta Mater. 61, 3808–3818.

Capolungo, L. Marshall, P.E. McCabe, R.J. Beyerlein, I.J. Tomé, C.N., 2009. Nucleation and growth of twins in Zr: A statistical study. Acta Mater. 57, 1351–1356.

Chapuis, A., Driver, J. H., 2011. Temperature dependency of slip and twinning in plane strain compressed magnesium single crystals. Acta Mater. 59, 1986–1994.

Christian, J. W., 2002. The theory of transformations in metals and alloys. Elsevier, Amsterdam.

Christian, J. W., Mahajant, S., 1995. Deformation Twining. Prog. Mater. Sci. 39, 1–157.

El Kadiri, H., Baird, J. C., Kapil, J., Oppedal, A. L., Cherkaoui, M., Vogel, S. C., 2013a. Flow asymmetry and nucleation stresses of $\{10\bar{1}2\}$ twinning and non-basal slip in magnesium. Inter. J. Plas. 44, 111–120.

El Kadiri, H., Barrett, C. D., Tschopp, M. A., 2013b. The candidacy of shuffle and shear during compound twinning in hexagonal close-packed structures. Acta Mater. 61, 7646–7659.

Jonsson, H., Mills, G., Jacobsen, K. W., 1998. Nudged elastic band method for finding minimum energy paths of transitions, in: B.J. Berne, G. Ciccotti, D.F. Coker (Eds.), Classical and Quantum Dynamics in Condensed Phase Simulations. World Scientific, Singapore.

Kelley, E. W., Hosdord, W. F. J. R., 1968. Plane-strain compression of magnesium and magnesium alloy crystals. Trans. Met. Soc. AIME 242, 5–13.

Khater, H., Serra, A., Pond, R., 2013. Atomic shearing and shuffling accompanying the motion of twinning disconnections in Zirconium. Phil. Mag. 93, 1279–1298.

Kihô, H., 1954. The crystallographic aspect of the mechanical twinning in metals. J. Phys. Soc. Jap., 9, 739–747.

Kim, J. H., Kim, D., Lee, Y. S., Lee, M. G., Chung, K., Kim, H. Y., Wagoner, R. H., 2013. A temperature-dependent elasto-plastic constitutive model for magnesium alloy AZ31 sheets. Inter. J. Plas. 50, 66–93.

Kresse, G., Furthmüller, J., 1996. Efficient iterative schemes for ab initio total-energy calculations using a plane-wave basis set. Phys. Rev. B 54, 11169–11186.

Kresse, G., Joubert, D., 1999. From ultrasoft pseudopotentials to the projector augmented-wave method. Phys. Rev. B 59, 11–19.

Lee, M. G., Kim, S. J., Han, H. N., 2010. Crystal plasticity finite element modeling of mechanically induced martensitic transformation (MIMT) in metastable austenite. Inter. J. Plas. 26, 688–710.

Lilleodden, E., 2010. Microcompression study of Mg (0001) single crystal. Scri. Mater. 62, 532–535.

Li, B., Ma, E., 2009a. Atomic shuffling dominated mechanism for deformation twinning in magnesium. Phys. Rev. Lett. 103, 035503.

Li, B., Ma, E., 2009b. Zonal dislocations mediating twinning in magnesium. Acta Mater. 57, 1734–1743.

Li, B., El Kadiri, H., Horstemeyer, M., 2012. Extended zonal dislocations mediating twinning in titanium. Phil. Mag. 92, 1006–1022.

Li, B., Zhang, X., 2014. Global strain generated by shuffling-dominated twinning. Scr. Mater. 71, 45–48.

Li, J., 2004. Transformation strain by chemical disordering in silicon carbide. J. Appl. Phys. 95, 6466–6469.

Li, J., 2007. The mechanics and physics of defect nucleation. MRS Bulletin 32, 151-159.

Li, W. B., Rieser, J. M., Liu, A. J., Durian, D. J., Li, J., 2015. Deformation-driven diffusion and plastic flow in amorphous granular pillars. Phys. Rev. E 91, 062212.

Liu, B., Wang, J., Li, B., Lu, L., Zhang, X., Shan, Z., Li, J., Jia, C., Sun, J., Ma, E., 2014. Twinning-like lattice reorientation without a crystallographic twinning plane. Nature comm. 5, 3297.

Luque, A., Ghazisaeidi, M., Curtin, W. A., 2013. Deformation modes in magnesium (0001) and $(01\bar{1}1)$ single crystals: simulations versus experiments. Modell. Sim. Mater. Sci. Eng. 21, 045010.

Luque, A., Ghazisaeidi, M., Curtin, W. A., 2014. A new mechanism for twin growth in Mg alloys. Acta Mater. 81, 442–456.

Mao, Y. W., Li, J., Lo, Y. C., Qian, X. F., Ma, E., 2015. Stress-driven crystallization via shear-diffusion transformations in a metallic glass at very low temperatures. Phys. Rev. B 91, 214103.

Monkhorst, H. J., Pack, J. D., 1976. Special points for Brillouin-zone integrations. Phys. Rev. B 13, 5188–5192.

Nie, Y., Xie, Y., 2007. Ab initio thermodynamics of the hcp metals Mg, Ti, and Zr. Phys. Rev. B 75, 174117.

Niezgoda, S. R., Kanjarla, A. K., Beyerlein, I. J., Tomé, C. N., 2014. Stochastic modeling of twin nucleation in polycrystals: An application in hexagonal close-packed metals. Inter. J. Plas. 56, 119–138.

Ogata, S., Li, J., Hirosaki, N., Shibutani, Y., Yip, S., 2004. Ideal shear strain of metals and ceramics. Phys. Rev. B 70, 104104.

Ogata, S., Li, J., Yip, S., 2002. Ideal pure shear strength of aluminum and copper. Science (New York, N.Y.) 298, 807–811.

Ogata, S., Li, J., Yip, S., 2005. Energy landscape of deformation twinning in bcc and fcc metals. Phys. Rev. B 71, 224102.

Oppedal, A., El Kadiri, H., Tomé, C., Kaschner, G., Vogel, S. C., Baird, J., Horstemeyer, M., 2012. Effect of dislocation transmutation on modeling hardening mechanisms by twinning in magnesium. Inter. J. Plas. 30-31, 41–61.

Ostapovets, A., Molnár, P., 2013. On the relationship between the "shuffling-dominated" and "shear-dominated" mechanisms for twinning in magnesium. Scr. Mater. 69, 287–290.

Perdew, J. P., Chevary, J. A., Vosko, S. H., 1992. Atoms, molecules, solids, and surfaces: Applications of the generalized gradient approximation for exchange and correlation. Phys. Rev. B 46, 6671–6687.

Proust, G., Tomé, C. N., Jain, A., Agnew, S. R., 2009. Modeling the effect of twinning and detwinning during strain-path changes of magnesium alloy AZ31. Inter. J. Plas. 25, 861–880.

Pulay, P., 1980. Convergence acceleration of iterative sequences. The case of SCF iteration. Chem. Phys. Lett. 73, 393-398.

Rasmussen, T., Jacobsen, K., Leffers, T., Pedersen, O., Srinivasan, S., Jónsson, H., 1997. Atomistic Determination of Cross-Slip Pathway and Energetics. Phys. Rev. Lett. 79, 3676–3679.

Sandlöbes, S., Friák, M., Zaefferer, S., Dick, A., Yi, S., Letzig, D., Pei, Z., Zhu, L. F., Neugebauer, J., Raabe, D., 2012. The relation between ductility and stacking fault energies in Mg and Mg-Y alloys. Acta Mater. 60, 3011–3021.

Serra, A., Bacon, D. J., Pond, R. C., 2010. Comment on "Atomic shuffling dominated mechanism for deformation twinning in magnesium". Phys. Rev. Lett. 104, 029603.

Shen, C., Li, J., Wang, Y., 2008. Finding critical nucleus in solid-state transformations. Metall. Mater. Trans. A-Phys. Metall. Mater. Sci. 39A, 976-983.

Sheppard, D., Xiao, P., Chemelewski, W., Johnson, D. D., Henkelman, G., 2012. A generalized solid-state nudged elastic band method. J. Chem. Phys. 136, 074103.

Sun, Q., Zhang, X., Tu, J., Ren, Y., Qin, H., Liu, Q., 2015. Characterization of basal-prismatic interface of twin in deformed titanium by high-resolution transmission electron microscopy. Phil. Mag. Lett. 95, 145–151.

Suresh, S., Li, J., 2008. Deformation of the ultra-strong. Nature 456, 716-717.

Tu, J., Zhang, X., Ren, Y., Sun, Q., Liu, Q., 2015. Structural characterization of $\{10\bar{1}2\}$ irregular-shaped twinning boundary in hexagonal close-packed metals. Mater. Char. 106, 240–244.

Tu, J., Zhang, X. Y., Lou, C., Liu, Q., 2013. HREM investigation of twin boundary and interface defects in deformed polycrystalline cobalt. Phil. Mag. Lett. 93, 292–298.

Wang, J., Li, J., Yip, S., Phillpot, S., Wolf, D., 1995. Mechanical instabilities of homogeneous crystals. Phys. Rev. B 52, 12627–12635.

Wang, J., Hirth, J. P., Tomé, C. N., 2009a. $(\bar{1}012)$ twinning nucleation mechanisms in hexagonal-close-packed crystals. Acta Mater. 57, 5521–5530.

Wang, J., Hoagland, R. G., Hirth, J. P., Capolungo, L., Beyerlein, I. J., Tomé, C. N., 2009b. Nucleation of a $(\bar{1}012)$ twin in hexagonal close-packed crystals. Scr. Mater. 61, 903–906.

Wang, L., Yang, Y., Eisenlohr, P., Bieler, T. R., Crimp, M. A., Mason, D. E., 2010. Twin nucleation by slip transfer across grain boundaries in commercial purity titanium. Metall. Mater. Trans. A: Phys. Metall. Mater. Sci. 41, 421–430.

Wang, J., Liu, L., Tomé, C. N., Mao, S. X., Gong, S. K., 2013a. Twinning and de-twinning via glide and climb of twinning dislocations along serrated coherent twin boundaries in hexagonal-close-packed metals. Mater. Res. Lett. 1, 81–88.

Wang, J., Yadav, S. K., Hirth, J. P., Tomé, C. N., Beyerlein, I. J., 2013b. Pure-shuffle nucleation of deformation twins in hexagonal-close-packed metals. Mater. Res. Lett. 1, 126–132.

Wang, J., Beyerlein, I. J., Tomé, C. N., 2014. Reactions of lattice dislocations with grain boundaries in Mg: Implications on the micro scale from atomic-scale calculations. Inter. J. Plas. 56, 156–172.

Wu, X., Liao, X., Srinivasan, S., Zhou, F., Lavernia, E., Valiev, R., Zhu, Y., 2008. New Deformation Twinning Mechanism Generates Zero Macroscopic Strain in Nanocrystalline Metals. Phys. Rev. Lett. 100, 095701.

Yoo, M. H., 1981. Slip, twinning, and fracture in hexagonal close-packed metals. Metall. Trans. A 12A, 409–418.

Yoshinaga, H., Horiuchï, R., 1963. On the nonbasal slip in magnesium crystals. Trans. Jap. Inst. Metals 5, 14–21.

Yu, C., Kang, G., Kan, Q., Song, D., 2013. A micromechanical constitutive model based on crystal plasticity for thermo-mechanical cyclic deformation of NiTi shape memory alloys. Inter. J. Plas. 44, 161–191.

Yu, Q., Qi, L., Chen, K., Mishra, R. K., Li, J., Minor, A. M., 2012. The nanostructured origin of deformation twinning. Nano lett. 12, 887–892.

Yu, Q., Zhang, J., Jiang, Y., 2011. Direct observation of twinning-detwinning-retwinning on magnesium single crystal subjected to strain-controlled cyclic tension-compression in [0001] direction. Phil. Mag. Lett. 91, 757–765.

Zecevic, M., Knezevic, M., Beyerlein, I. J., Tomé, C. N., 2015. An elasto-plastic self-consistent model with hardening based on dislocation density , twinning and de-twinning : Application to strain path changes in HCP metals. Mater. Sci. Eng. A 638, 262–274.

Zhao, P., Li, J., Wang, Y., 2013. Heterogeneously randomized STZ model of metallic glasses: Softening and extreme value statistics during deformation. Inter. J. Plas. 40, 1–22.

Zhu, Y., Liao, X., Wu, X., 2012. Deformation twinning in nanocrystalline materials. Prog. Mater. Sci. 57, 1–62.

Zhu, T., Li, J., 2010. Ultra-strength materials. Prog. Mater. Sci. 55, 710–757.

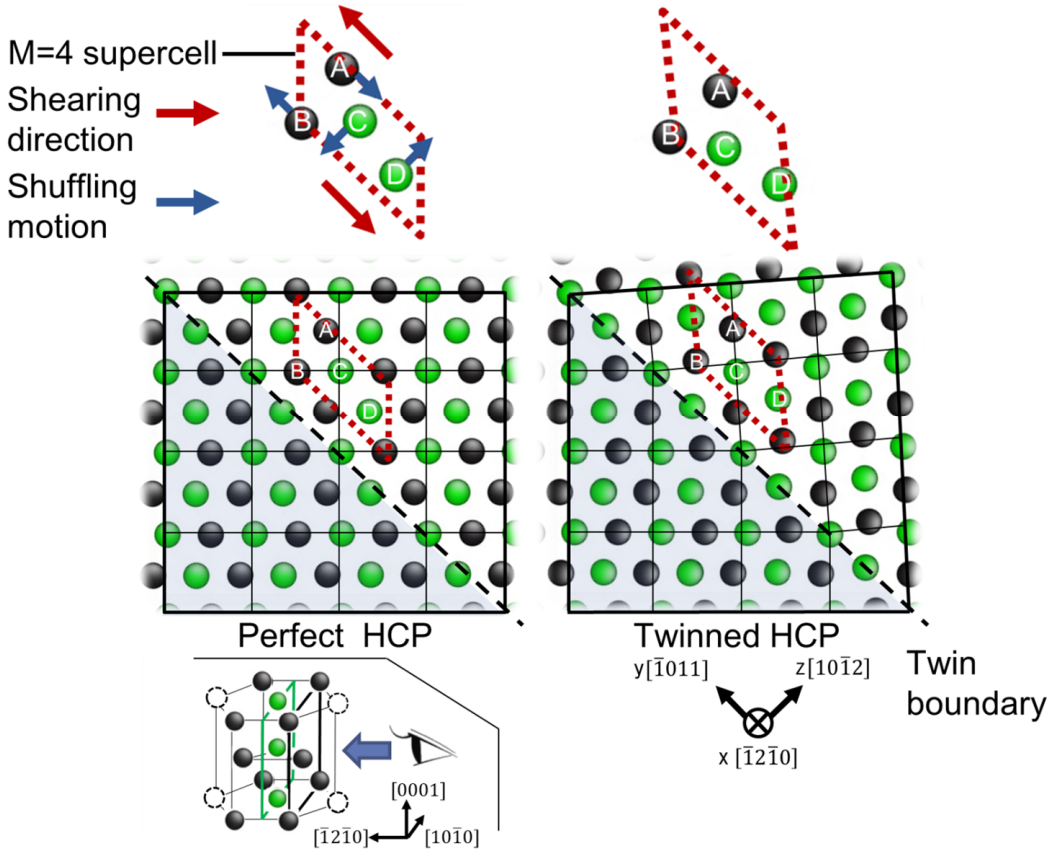

Figure 1: Atomic arrangements and four-atom supercell shape of perfect HCP and twinned HCP configurations viewed from $[1\bar{2}10]$. The different colored atoms represent atoms in each of the $(1\bar{2}10)$ atomic planes. The DFT four-atom supercell, which includes atoms A, B, C, and D, are indicated by a broken red line. The $M = 4$ supercell (see text for the details) and shearing direction and typical atomic shuffling motion when I defined in eqn. 5 is increased in the supercell are also shown.

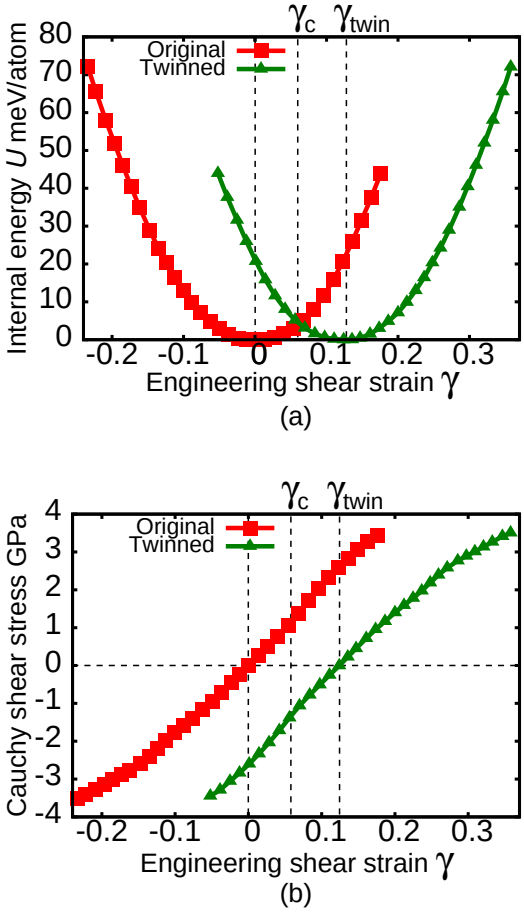

Figure 2: Supercell internal energy (a) and, Cauchy shear stress (b) with respect to engineering shear strain γ. The shear deformation is applied to two different initial supercell atomic configurations: "original" (red plots) and "twinned" (green plots). An energy crossover occurs at $\gamma = \gamma_c (= 0.062)$.

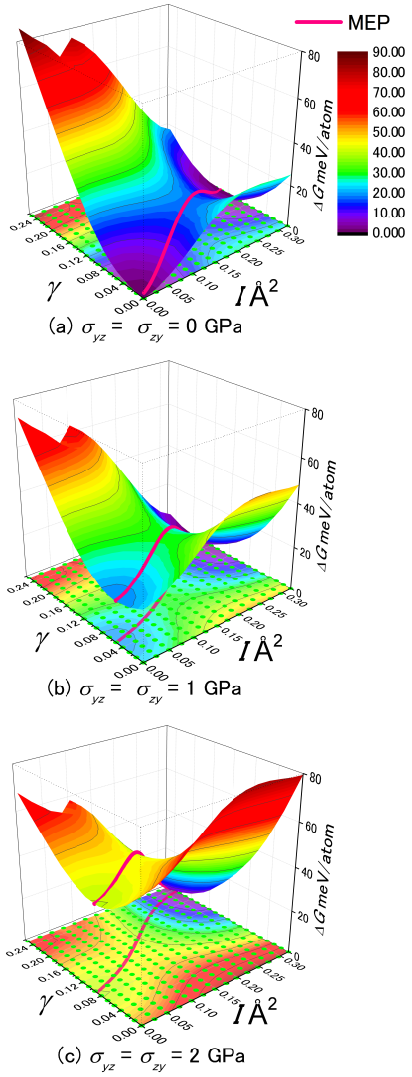

Figure 3: Gibbs energy distribution $\Delta G(\gamma, I)$ at different levels of external shear stress $\sigma_{yz} = \sigma_{zy} = 0$ GPa (a), 1 GPa (b), 2 GPa (c). The red curves represent the MEPs of the deformation twinning processes. The raw data are available as supplemental information "Internal_ene_dist_U_data.txt" and "External_work_W_data.txt".

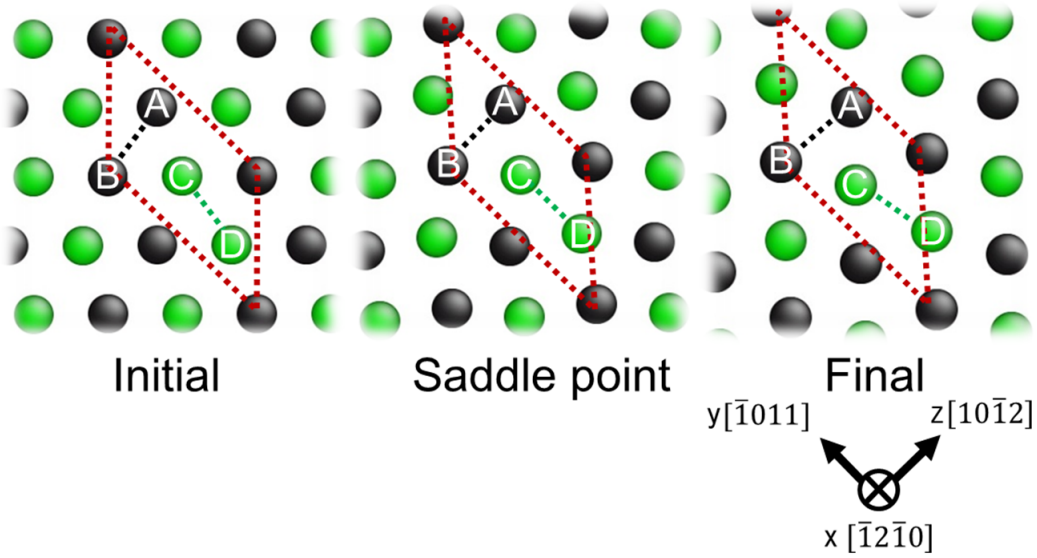

Figure 4: Atomic configuration change along the MEP at $\sigma_{yz} = \sigma_{zy} = 0$ GPa. A staggered rotation of the A-B and C-D atomic bonds can be observed. See also supplemental movie Suppl_movie.pptx.

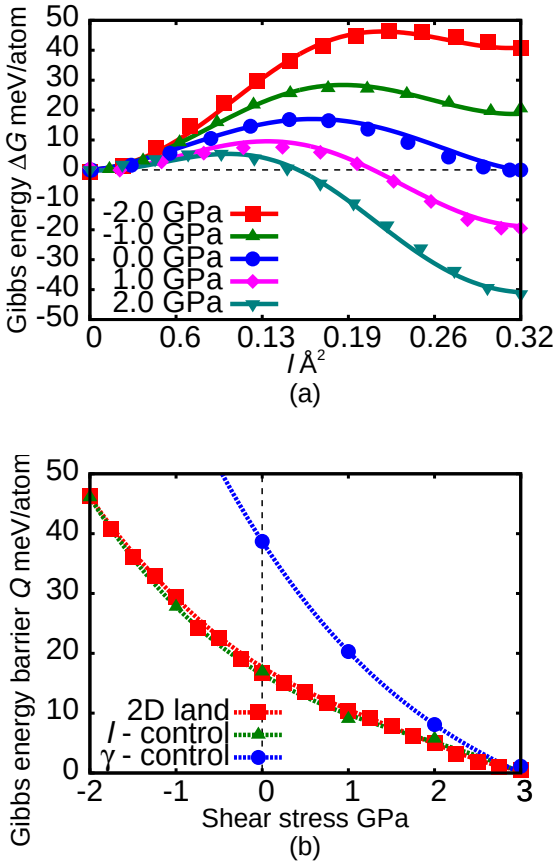

Figure 5: Gibbs energy variation along the MEP (a) and the energy barrier change with respect to external shear stress (b). In (a), the solid curves and dots represent results obtained from the Gibbs energy landscape and direct NEB analysis, respectively. In (b), the square, triangular, and circular dots represent the Gibbs energy barriers obtained from the two-dimensional Gibbs energy landscape (2D land), I-control NEB, and γ-control NEB, respectively. The lines are intended to guide the eye.

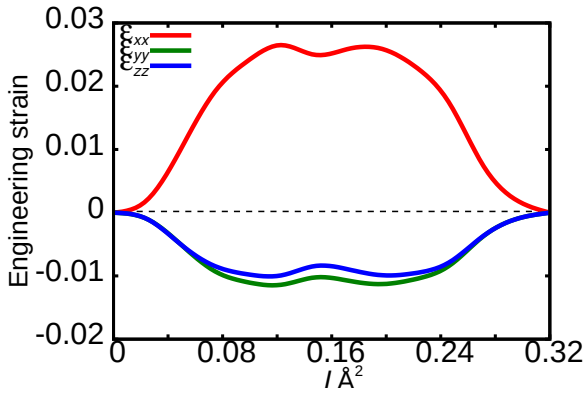

Figure 6: The change in engineering strain components, $\varepsilon_{xx}, \varepsilon_{yy}, \varepsilon_{zz}$, along the MEP at $\sigma_{yz} = \sigma_{zy} = 0$ GPa. Note that always $\gamma_{xy} = \gamma_{zx} = 0$.